

2 **Investigations into the Tectonic Faults on**  
3 **Magadi Geothermal Field Using Ground and**  
4 **Aeromagnetic Data**

5  
6 **A. A. Komolafe<sup>1,\*</sup>, Z. N. Kuria<sup>2</sup>, T. Woldai<sup>3</sup>, M. Noomen<sup>3</sup>, A. Y. B. Anifowose<sup>1</sup>**

7 <sup>1</sup>Department of Remote Sensing and Geoscience Information System, Federal University of  
8 Technology, Akure, Nigeria

9 <sup>2</sup>Department of Geology, University of Nairobi, Kenya

10 <sup>3</sup>University of Twente, ITC, Enschede, Netherlands

11  
12  
13

14 **ABSTRACT**

Lake Magadi area of the Kenya Rift is characterized by faulting, tectonic activities and geothermal resources. The geothermal potential of the graben in the southern part of the lake was investigated using magnetic methods (ground and airborne). This was done to determine the geometry of tectonic faults and ascertain their influence on the flow of hot springs, which are manifested on the surface. Five N-S faults were identified for ground investigation using ground magnetic survey. Magnetic data were processed using vertical derivatives, analytical signal and Euler deconvolution. The faults were further mapped with aeromagnetic data using 2D Euler deconvolution. Magnetic derivative grids and profiles revealed subsurface faulting/tectonic activities up to a depth of 400m and the presence of fluid-filled zones within the basin, which are marked by the absence of magnetic sources. A deeper investigation into the lineaments from the aeromagnetic data showed that the surface faults extend into a depth of 7.5 km in the subsurface. The alignment of magnetic sources at the rift axis showed that these faults are probably the parallel faults which bound the basin/graben to the west and to the east. The N-S faults structures in the south of the lake serve as conduits for fluids which support the upward flow of the hydrothermal fluid along its margin.

15

16 **Keywords:** *Lake Magadi, Magnetics, Tectonics, Geothermic, Kenya Rift*

17

18

19 **1. INTRODUCTION**

20 The roles of faults and fractures on crustal fluids have been of major interest in earth sciences, including  
21 geology, seismology, hydrogeology and petroleum geology [2]. The static and dynamic effects of different  
22 stresses on rocks often produce change in rock mass such as fractures, faults and in general permeability  
23 which in turn control the flow of fluids in the earth crust. [3] define fractures and faults are planes of tensile  
24 or shear failure at microscopic to regional scales in brittle rocks. These faults and fractures are developed  
25 mostly in competent rocks within the earth crust. In case of fractures, they are usually developed when  
26 the stress applied exceeds the elastic limit of the rock [3]. These two deformations are of great  
27 importance in crustal fluid distributions and control. The movement of crustal fluids (in this case,  
28 hydrothermal) to the surface from the reservoir rock depends of the pressure, temperature and most  
29 importantly the presence of active faults and fractures in the subsurface which are extended to the  
30 surface.

31

\* Tel.: +2348037899856.

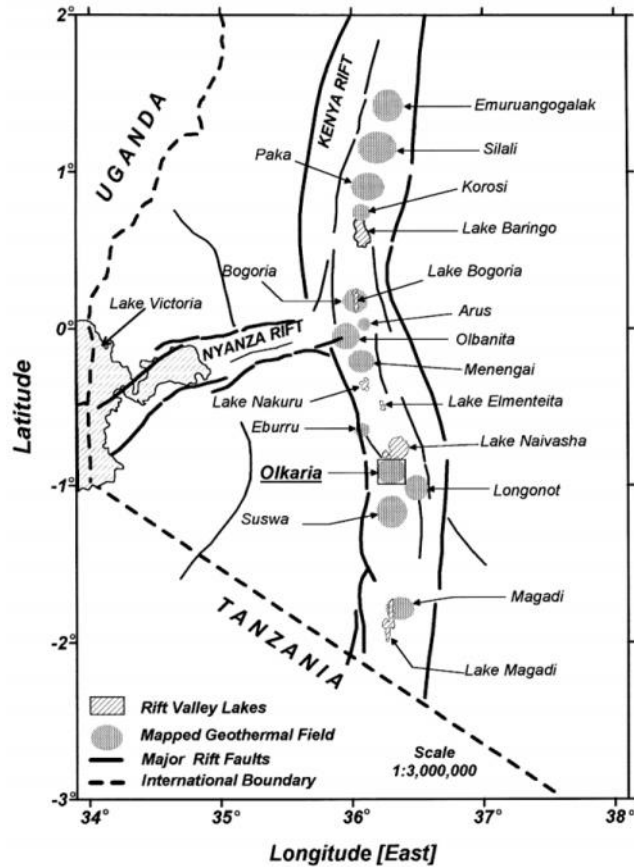
E-mail address: [aakomolafe@futa.edu.ng](mailto:aakomolafe@futa.edu.ng)

32 Geothermal resources, according to [4] are generally associated with tectonically active region which are  
33 generated as a result of temperature differences between the different parts of the asthenosphere (below  
34 the lithosphere) where convective movement are formed. This slow convective movement is said to be  
35 maintained by the radioactive elements and heat from the deepest part of the earth. The less dense deep  
36 hotter rocks tends to rise with the movement towards the surface while the colder but heavier rocks close  
37 to the surface tend to sink, re-heat and rise again. Generally, geothermal system is made up of the heat  
38 source, the reservoir, the recharge area and the connecting paths such as faults and fractures through  
39 which fluids percolates to the reservoir (the host rock) and in most cases are escaped to the surface as  
40 fumaroles and hot springs. The heat source is often assumed to be magmatic intrusion that has reached  
41 shallow depths (5-10km) [4]. The reservoir rocks are permeable rocks through which fluids circulates and  
42 extracts heat from the heat source. This is overlain by impermeable rocks and is connected to a surficial  
43 recharge area. Through fractures, meteoric water replaces or partly replaces the fluids which escape from  
44 the reservoirs as springs or during drilling.

45  
46 Geothermal activities are associated with most parts of the Kenyan rift valley. The warm and hot springs  
47 are mostly connected to the lakes through various conduits [5]. Geothermal manifestations have been  
48 indentified at different locations in the study area (Figure 1), the most active and currently producing  
49 being the Olkaria geothermal field the northern part [1]. It exists within an old caldera complex, with  
50 surface manifestations in form of hot springs. It is associated with N-S normal faulting as observed by [1]  
51 in the southern part of the rift (Magadi). Lake Magadi water is mostly derived from underground hot water  
52 inflow with a continuous recharge from the surface waters [5-6]. Unlike some other geothermal regions  
53 where the reservoirs containing hot fluids have to be penetrated during exploitation, geothermal  
54 resources around Lake Magadi are clearly manifested on the surface in the form of hot springs and trona  
55 deposit along the lake margin and in the lake respectively. These surface manifestations of the hot  
56 springs have been attributed to continuous tectonic activities and the presence of various faulting systems  
57 in the area [6-7]. The role of N-S faults in the south of Lake Magadi as major conduits for geothermal  
58 resources and the deposition of trona in the lake have been proposed by [6] but not yet investigated,  
59 hence the focus of this study in order to know the flow paths of hydrothermal fluids with the aim of  
60 understanding the geothermal potentials.

61  
62 [8] Investigated the proposed influence of the tectonic faults at Lake Magadi using geoelectric method.  
63 Their investigations revealed an upward flow of saline hot water to the surface via the fault splay; this was  
64 revealed by the relatively low resistivity within the profile. To further probe the claim, ground magnetic  
65 method with constraint from the airborne magnetic was applied to investigate the geometry of the N-S  
66 faults in the south of Lake Magadi and determine their influence on the expression of geothermal  
67 resources such as hot springs and trona deposits.

68  
69 Magnetics method is very effective in studying structures and delineating depth to heat source in  
70 geothermal environments [8-10]. This study employs the use of magnetic methods (ground and airborne)  
71 to investigate the geometry of the N-S faults in the south of Lake Magadi and determine their influence on  
72 the expression of geothermal resources such as hot springs and trona deposits.



73  
 74 Figure1: Location of significant geothermal areas in the Kenya Rift  
 75 Valley (Source: [1]).  
 76

77 **1.2. THE STUDY AREA**

78  
 79 Lake Magadi area is the southernmost part of Kenya Rift, 120km southwest of Nairobi and 20km north of  
 80 the Tanzanian border. It is located within Latitudes 1°40'S and 2°10'S, and Longitudes 36°00'E and  
 81 36°30'E, characterized by a flat rift floor [11] (Figure 2). The approximately 100km<sup>2</sup> size lake is recharged  
 82 by saline hot springs (between 26°C and 86°C) along the lake margins [6]. Most of the hot springs lie  
 83 along the north-western and southern shorelines of the lake. The lake comprises of trona deposit  
 84 (Na<sub>2</sub>CO<sub>3</sub>.NaHCO<sub>3</sub>.2H<sub>2</sub>O) about 40m thick, covering about 75km<sup>2</sup> resulting from the concentration of  
 85 different water sources, especially hydrothermal fluid [6]. According to [12] after a chemical analysis of  
 86 collected waters, Magadi trona results from the evaporated concentration and mixing of waters from three  
 87 sources namely dilute surface inflow, relatively deep hot and concentrated groundwater reservoir, and  
 88 cold concentrated surface brine. An analysis of the water revealed five distinct hydrologic stages in the  
 89 evolution of the water compositions viz: i) the dilute stream flow, ii) dilute ground water, iii) saline ground  
 90 water (or hot springs reservoir), iv) saturated brines, and v) residual brines [6]. The active alkaline  
 91 volcanoes in the area through hydrothermal systems circulation supply the saline (alkaline brine) hot  
 92 springs. For the purpose of this study, sampling points located close to the hot springs in the southern  
 93 part of the Lake were selected (Figure 2).  
 94  
 95  
 96  
 97  
 98  
 99  
 100

101  
102  
103  
104  
105  
106  
107  
108  
109  
110  
111  
112  
113  
114  
115  
116  
117  
118  
119  
120  
121  
122  
123  
124  
125  
126  
127  
128  
129  
130  
131  
132  
133  
134  
135  
136  
137  
138  
139  
140  
141  
142  
143  
144  
145  
146  
147  
148  
149  
150  
151

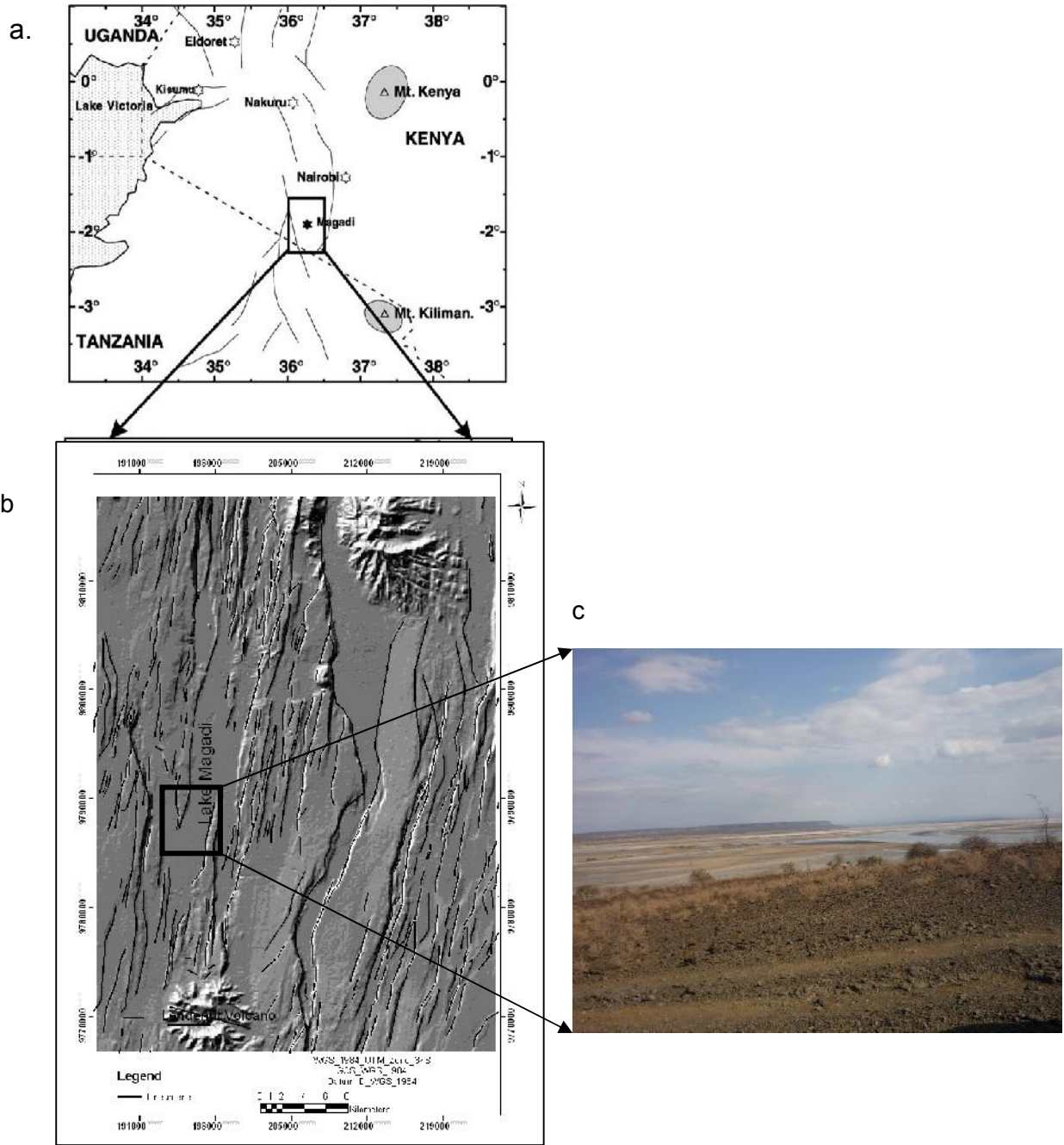


Figure 2 (a) Geographic location of Magadi area (Adapted from [11], (b) Lineament map of Lake Magadi overlain on SRTM DEM (c) The study area and associated springs.

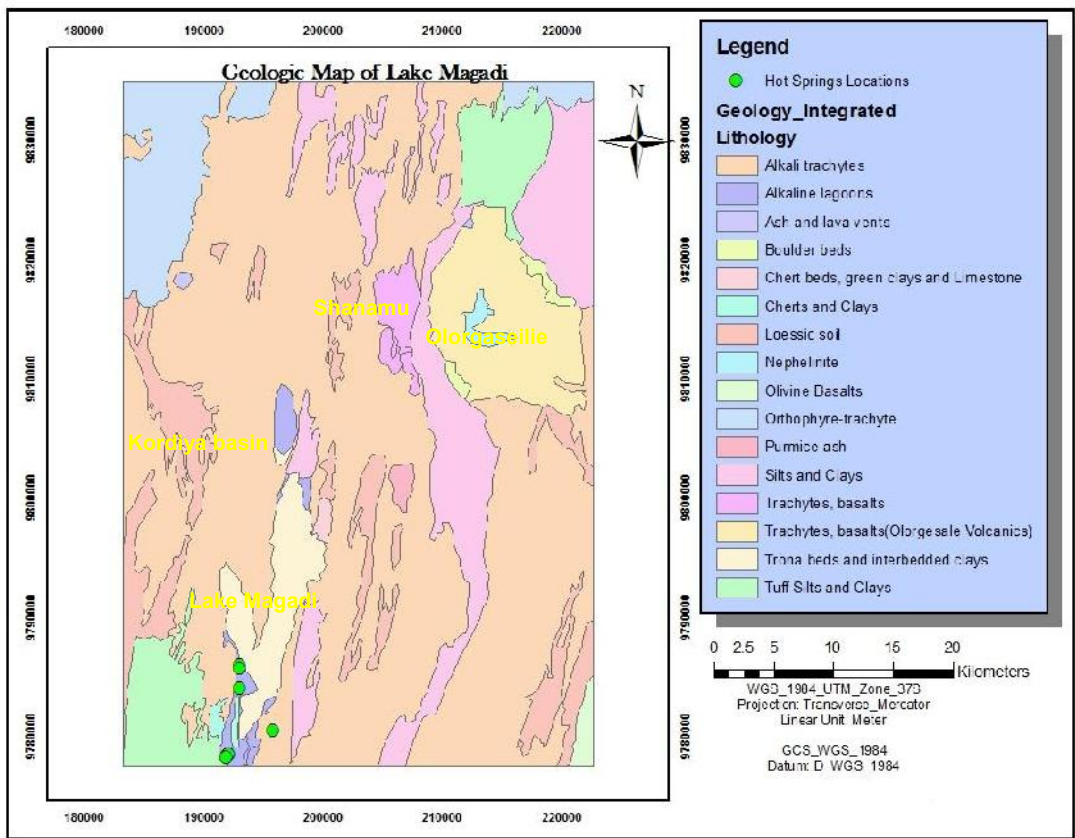
### GEOLOGY OF LAKE MAGADI

[13] described the geology of Lake Magadi as being made up of mostly Archean to early Paleozoic crystalline basement rocks and rift-related volcanics and sediments (Figure 3). The rock succession can be grouped into Precambrian metamorphic rocks, Plio-to Pleistocene volcanic rocks, and Holocene to Recent lake and fluvial sediments [11]. The oldest rocks in the area are the quartzites, gneisses and schists of Archean age. The extrusion of alkali trachytes within the lake as explained by [14] and [15] occurred in the Pleistocene age. In the southern and northern ends of the Lake Magadi area, there is a deposition of irregular interbedded chert rocks which consists of silicified bedded clays on top of alkali

\* Tel.: +2348037899856.

E-mail address: [aakomolafe@futa.edu.ng](mailto:aakomolafe@futa.edu.ng)

152 trachytes [11, 16]. This is unconformably overlain by a thin layer of lake beds known as the Oloronga  
 153 beds, followed by a series of sub-parallel faulting system that resulted in the formation of the Lake Magadi  
 154 rift floor. The formation of the Quaternary sediments exists within a fault-bounded basin.  
 155 An integrated seismic, drill hole data and gravity model by [17] revealed sediments and volcanic complex  
 156 at the rift floor adjacent to Nguruman escarpment. Their model explained the crustal structure of Lake  
 157 Magadi as having basement rocks at the bottom which are exposed at the western (Tanzanian craton)  
 158 and eastern (Mozambique belt) flanks, and overlain by Pliocene to Miocene volcanic and sedimentary  
 159 rocks. The Rift has been discovered to exist in the boundary between the Archean Tanzanian craton and  
 160 Neoproterozoic Mozambique belt, which is characterized by a complex fault zone [13]. The tectonic  
 161 settings and structures of Lake Magadi are influenced by three factors, namely stable Tanzanian Craton,  
 162 Aswa shear zones, and southern fringes of the Kenya dome [18]. The four major fault sets associated  
 163 with the Kenya rift (normal N-S fault, dextral NW-SE fault, strike slip ENE-WSW fault and sinistral NE-SW  
 164 fault) are revealed at Lake Magadi (Figure 2).  
 165



192 Figure 3: Simplified Geology map of the study area after [14]

193 **2. METHODOLOGY**

194

195 **2.1. GROUND MAGNETIC DATA**

196

197 Ground and airborne magnetic methods were adopted to study the subsurface geometry of the tectonic  
 198 faults and their influence of the geothermal resources in Lake Magadi. Since it measures the magnetic  
 199 field intensity of the Earth, the magnetic technique is capable of mapping subsurface structures such as  
 200 faults, grabens, horsts and lithology. According to [19], lithology controls magnetic properties through  
 201 mineralogy, and sharp variation in rock properties generally coincides with lithological contacts.  
 202 Generally, igneous and metamorphic rocks show significant magnetic properties while sedimentary rocks  
 203 are mostly non-magnetic [20].

\* Tel.: +2348037899856.

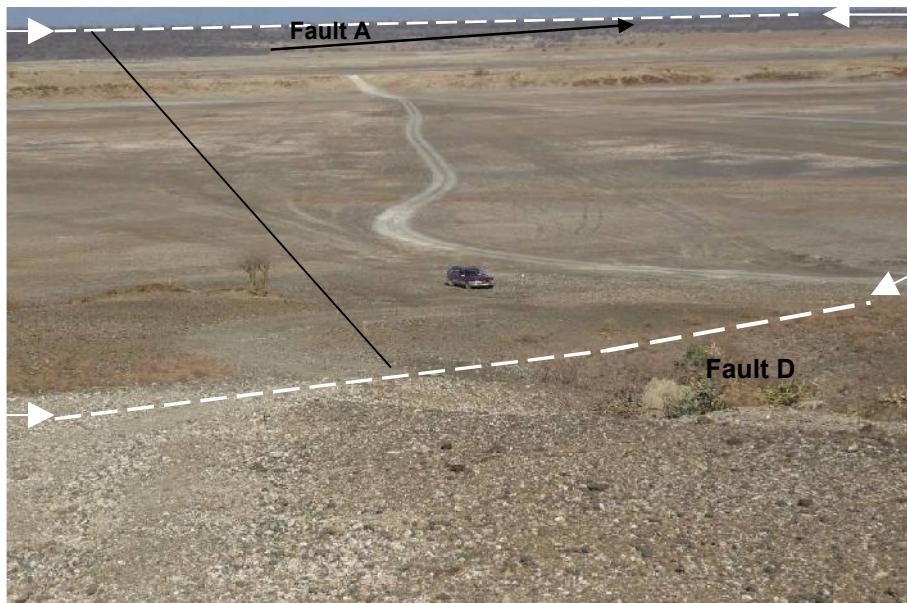
E-mail address: [aakomolafe@futa.edu.ng](mailto:aakomolafe@futa.edu.ng)

204  
205  
206  
207  
208  
209  
210  
211  
212  
213  
214  
215  
216  
217  
218  
219  
220  
221  
222  
223  
224  
225  
226  
227  
228  
229  
230  
231  
232  
233

The existence of faults and fractures in the geologic units creates magnetic variations which generate magnetic anomalies. [21] highlight the importance in mapping hydrothermal alteration zones. This is because most magnetic rocks must have been altered and converted from magnetite to pyrite, which in turn results in lower magnetic anomaly than the unaltered zones. In general, the presence of fluid within the faults and fractures would reduce or have no magnetic response. The geometry of subsurface structures can be constructed from magnetic profiles data using various inversion processes. The anomaly due to the near surface and deep source can be enhanced using vertical derivative and upward continuation respectively. Depth to magnetic sources and geometry of the structures can be estimated from Euler's deconvolution method as applied in this study.

Geometrics 856 Proton Precession Magnetometer was used for the magnetic survey. It is made up of six-digit display of the magnetic field and three digit displays of station, line number and signal strength, and it measures the absolute value of total magnetic field to a resolution of 0.1nT with accuracy of 0.5nT. the equipment is used in various field applications such as geological mapping, mining and location of magnetic materials. Geometrics 856 Proton Precession Magnetometer uses 9 D cell industrial grade batteries and it is connected to magnetic coils mounted on the pole for measurement.

Five fault systems referred to as A, B, C, D, and E (from west to east) assumed to be the major fluid conduits in the south of the lake, within the basin were identified for ground investigation (Figures 4 and 5). Major faults around Lake Magadi are the normal N-S fault, dextral NW-SE fault; strike slip ENE-WSW fault and sinistral NE-SW fault [11, 16]. The N-S faults are well pronounced in the area and are suspected to be the oldest faults in the Lake Magadi area while the youngest are the NE - NW faults. Data were collected perpendicularly to the strike of the four (4) structures in the south of Lake Magadi. Four profiles (P1, P2, P3 and P4) were established to cover a lateral distance of 2.3 km running west–east direction across the hot springs, separated by 330, 330 and 360 meters respectively and located along the lake margins (Figure 5). The profiles cover the area marked by Faults A and D (Figure 4). The latter faults are defined by steep fault scarps. Magnetic measurement was taken at every 25m station along the traverse (west-east direction) with the base station readings taken at every one hour for diurnal correction at the same position where the previous data was taken.



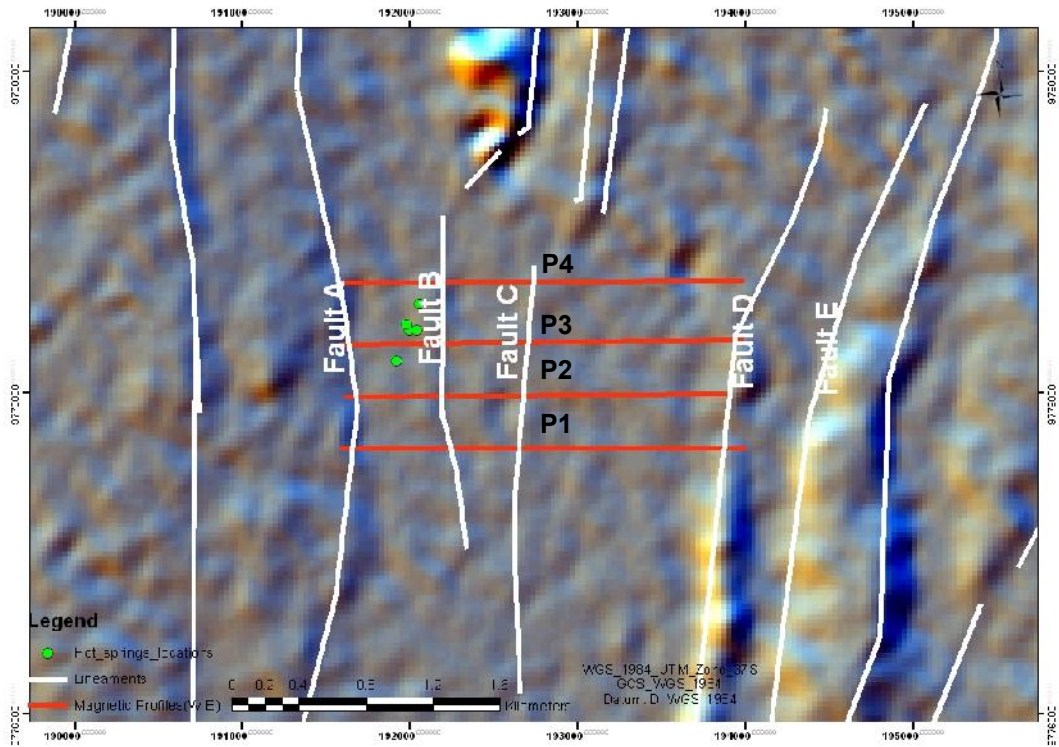
234  
235  
236  
237  
238

Figure 4. Field photo showing the magnetic profile extent from Fault A to Fault D (on a west-east direction); the black arrow indicates the North.

239  
240  
241  
242  
243  
244  
245  
246



247  
248  
249  
250  
251  
252  
253  
254  
255  
256  
257  
258  
259  
260  
261  
262  
263  
264  
265  
266



267  
268  
269

Figure 5 (a): Field photo showing the hot springs along the lake margin between Faults A and B. (b): Hill-shaded AsterDEM showing the magnetic profiles across the major faults in the study area.

## 2.2. DATA PROCESSING

### Diurnal Variation Correction

Variation of Earth's magnetic field with time, due to the rotation of the earth and with respect to the solar wind, which may last several hours to one day, is called diurnal variation [22]. In order to correct for drift or diurnal effect in the magnetic readings, a base station within the four magnetic profiles, assumed to be free from magnetic noise was selected. Repeated readings were taken every one hour of the magnetic measurement for the drift correction. Thereafter, the diurnal effect was calculated and the magnetic data

\* Tel.: +2348037899856.  
E-mail address: [aakomolafe@futa.edu.ng](mailto:aakomolafe@futa.edu.ng)

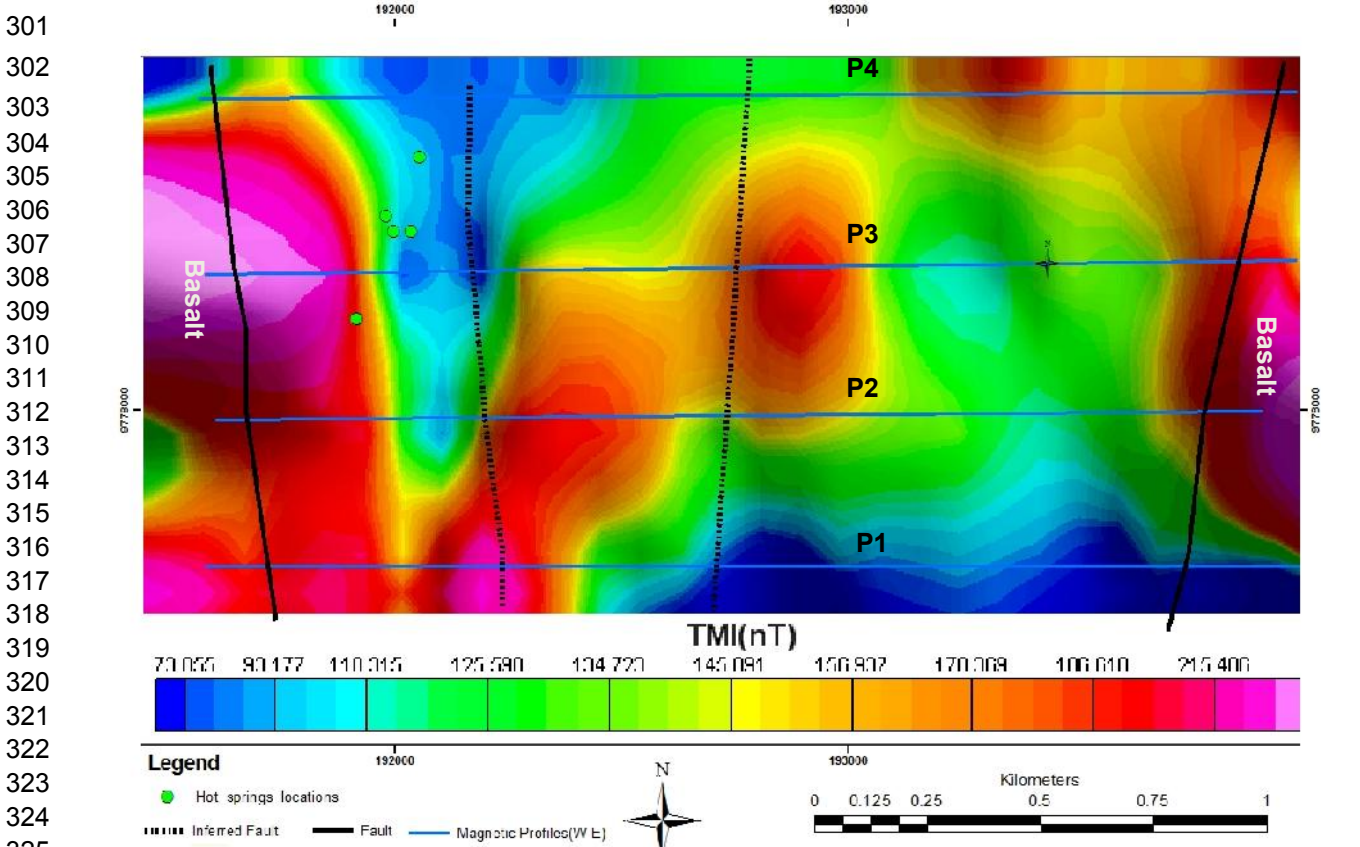
278 were filtered. Noise due to secular change or epoch was considered negligible because consistent  
279 measurements were taken at the base station every hour [23].  
280

### 281 Calculation and Removal of the Geomagnetic Field

282 Magnetic survey involves measurement of the sum of magnetic field produced by both local and regional  
283 magnetic fields. The regional magnetic field, often referred to as geomagnetic field needed to be  
284 subtracted from the acquired total magnetic field to obtain the magnetic field anomaly caused by the local  
285 source. The geomagnetic field was subsequently calculated using the International Geomagnetic  
286 Reference Frame (IGRF) Model 2005 in Geosoft™ Oasis Montaj. This model is calculated based on the  
287 dates, elevation and geographical locations (Latitudes and Longitudes) of the observed magnetic data  
288 with the generated average geomagnetic field of 33430nT, inclination of -26.2° and declination of 0.03°.  
289 The IGRF values were subtracted from the observed magnetic values for each station to determine the  
290 residual magnetic field due to anomalous contributions from local magnetic sources in the area.  
291

### 292 2.3. Data Enhancements

293 The corrected magnetic data were presented in grid forms for visualization and further enhancements.  
294 The total magnetic intensity (TMI) data were gridded using minimum curvature gridding method with 50m  
295 cell size, having the four faults and hot-springs locations overlaid (Figure 6). A minimum curvature surface  
296 is the smoothest possible surface that will fit the given data values [24]; It smoothes two straight-line  
297 segments by using the Ratio Factor. This gridding method is very effective in the interpolation of gridded  
298 points. For effective interpretation of the obtained magnetic data, further enhancements were carried out  
299 using various filtering techniques.  
300



301  
302  
303  
304  
305  
306  
307  
308  
309  
310  
311  
312  
313  
314  
315  
316  
317  
318  
319  
320  
321  
322  
323  
324  
325  
326 Figure 6: Gridded residual ground Total Magnetic field Intensity (TMI) for the four  
327 profiles showing hot springs and faults locations.  
328  
329

330  
331  
332  
333  
334  
335  
336  
337  
338  
339  
340  
341  
342  
343  
344  
345  
346  
347  
348  
349  
350  
351  
352  
353  
354  
355  
356  
357  
358  
359  
360  
361  
362  
363  
364  
365  
366  
367  
368  
369  
370  
371

### Vertical Derivatives

Vertical derivatives of magnetic data generally aid the interpretation process as it enhances and sharpens geophysical anomalies. This filtering method is effective in enhancing anomaly due to shallow sources; it narrows the width of anomalies and very effective in locating source bodies more accurately [25]. Vertical derivative was done by applying low-pass filters to remove high-wavelength, thereby enhancing low-wavelength component of the magnetic spectrum. The vertical derivative of the total magnetic Intensity was derived in Geosoft™ Oasis software as shown in Figure 7.

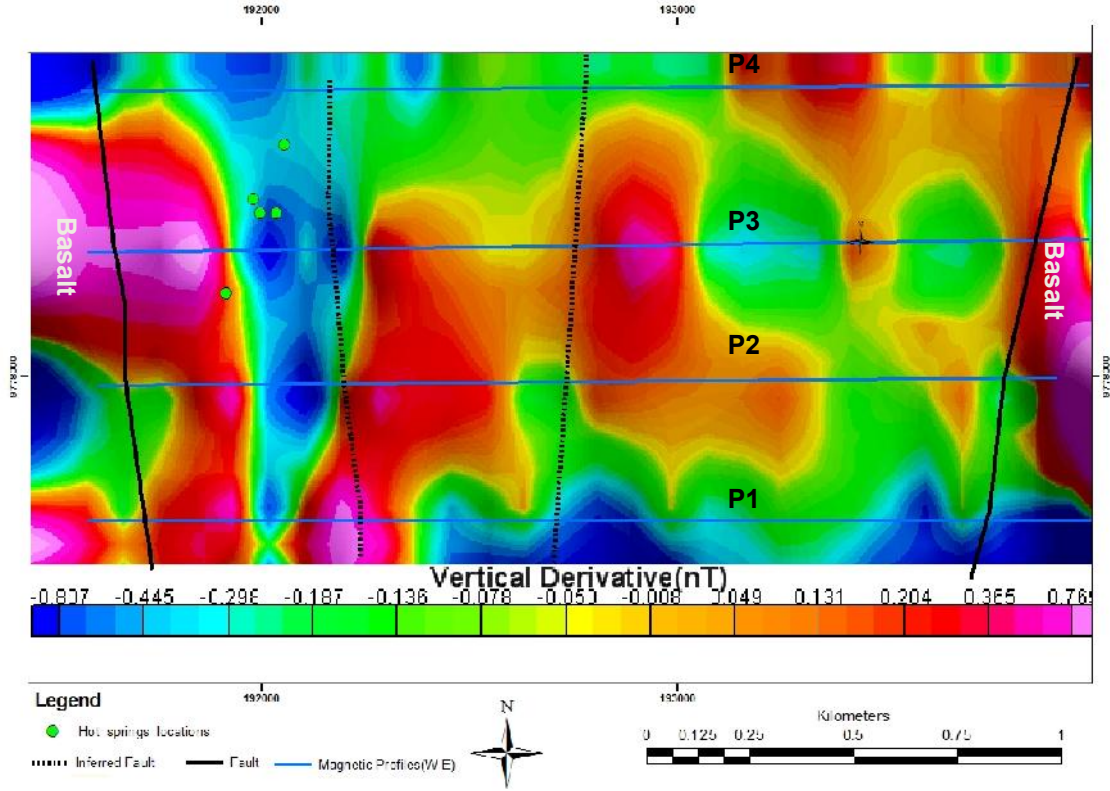


Figure 7: Colour-shaded vertical derivative of the magnetic field intensity showing the shallow magnetic sources.

### Analytical Signal

Absolute analytic signal according to [26] can be defined as the square root of the squared sum of the vertical and horizontal derivatives of the magnetic field (Equation 1)

$$AS = \sqrt{\delta x.\delta x + \delta y.\delta y + \delta z.\delta z} \quad \text{Equation (1)}$$

Where  $\delta z$  is the vertical derivative,  $\delta x$  and  $\delta y$  are the horizontal derivatives and AS is the analytical signal.

The advantage of this method of magnetic data enhancement is that its amplitude function is an absolute value and does not need assumption of the direction of source body magnetization [27]. Analytical signal can be used to locate the edges of remanently magnetized bodies, reveal anomalous textures and highlight discontinuities [28]. The analytical signal derived from the obtained magnetic data enhances the edges of the major structures in the study area (Figure 8).

\* Tel.: +2348037899856.  
E-mail address: [aakomolafe@futa.edu.ng](mailto:aakomolafe@futa.edu.ng)

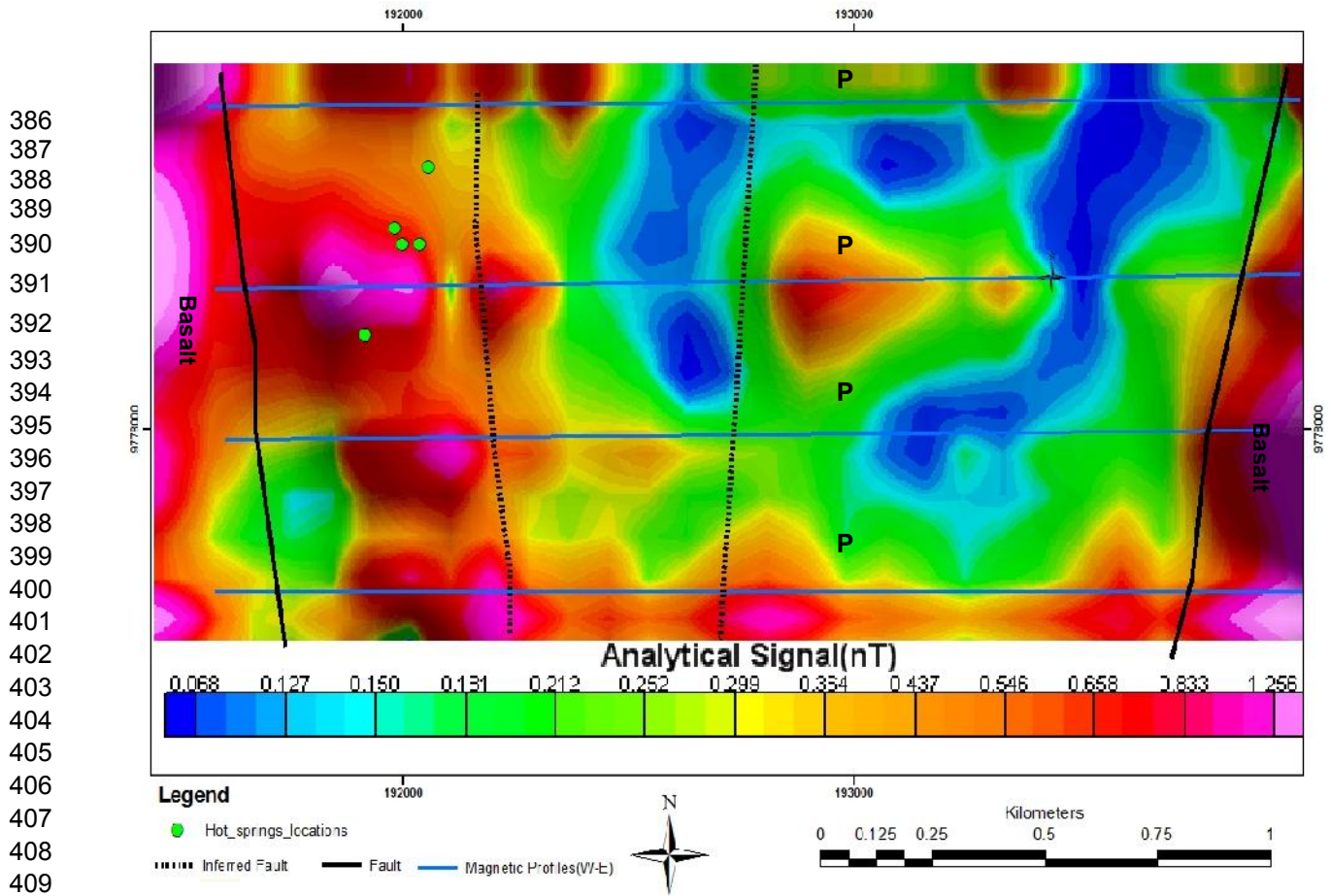


Figure 8: Colour -shaded Analytical signal maps of the four profiles

## Euler Deconvolution

Euler deconvolution is an inversion method for estimating location and depth to magnetic anomaly source. It relates the magnetic field and its gradient components to the location of the anomaly source with the degree of homogeneity expressed as a structural index and it is the best suited method for anomalies caused by isolated and multiple sources [29]. The structural index (SI) is a measure of the fall-off of the field with distance from the source. Euler deconvolution is expressed in Equation (2) as:

$$(x - x_0)\delta T / \delta x + (y - y_0)\delta T / \delta y + (z - z_0)\delta T / \delta z = N(B - T) \quad \text{Equation (2)}$$

where  $(x_0, y_0, z_0)$  is the source position of a magnetic source whose total field  $T$  is measured at  $x, y, z$ , while  $B$  is the regional value of the total field, and  $N$  is expressed as the structural index (SI), a measure of the rate of change with distance of the potential field, depending on the geometry of the source [29].

Estimating depth to magnetic anomaly using Euler deconvolution involves the following: i) Reduction to the pole; ii) Calculation of horizontal and vertical gradients of magnetic field data, calculated in frequency domain; iii) choosing window sizes; and iv) structural index, e.g. contact, dike and point [29]. In general, the desired structural indices are chosen with the window size for depth determination. This is set based on the anomaly of interest. In this study, both 3D and 2D Euler deconvolution were adopted for both the gridded and profile data respectively.

## 2D Euler Deconvolution

Two-dimensional Euler deconvolution was generated from the software developed by [30] for constraining the subsurface geometry along the profile lines. The software requires magnetic parameters

\* Tel.: +2348037899856.

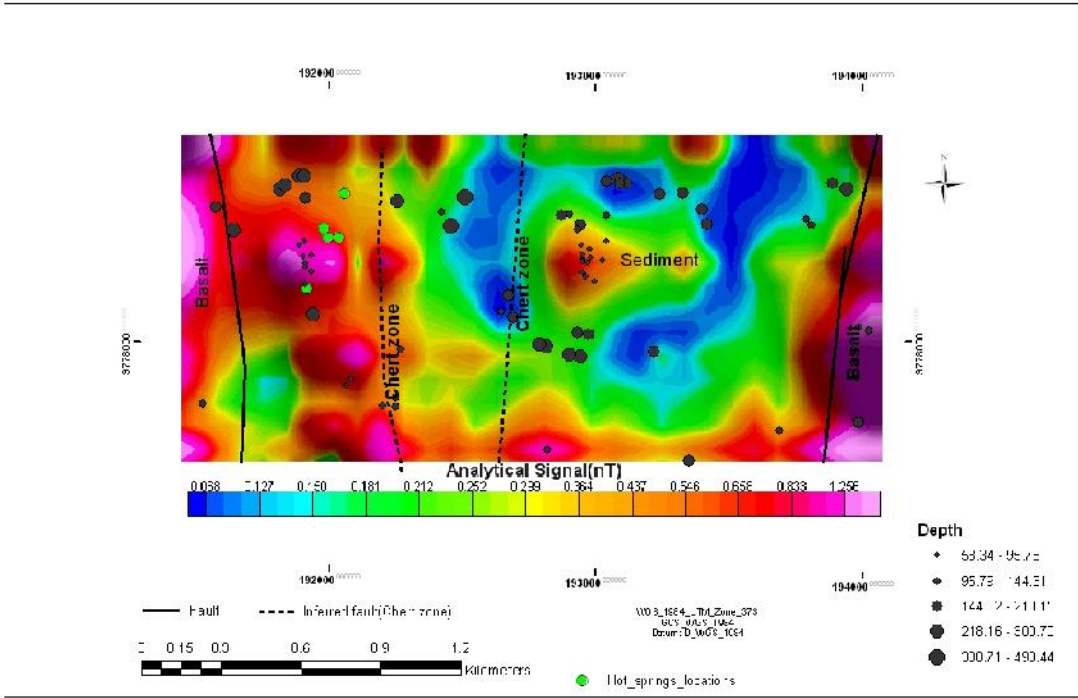
E-mail address: [aakomolafe@futa.edu.ng](mailto:aakomolafe@futa.edu.ng)

438 such as the geomagnetic field, survey locations, inclinations and declination angles. Two columns with a  
 439 space delimited ASCII file are required for input; the first column is the magnetic station locations while  
 440 the second column is the corrected magnetic field values. The results of the IGRF was used as the inputs  
 441 for this process, i.e. geomagnetic field intensity of 33430nT, inclination of -26.2° and declination of 0.03°.  
 442 Similar to the 3D Euler deconvolution, the structural indices and the Euler window size must be selected.  
 443 In this research, a window size of 13, 110m X-separation and 55m Y separation were adopted. To better  
 444 constrain the subsurface geology, 1.0 structural index (steep contact) which is an indication of faults  
 445 contacts were plotted for all the traverses; these are shown in Figures 11- 14 respectively.

446  
 447 **3D Euler Deconvolution**

448 3D Euler deconvolution was performed on the total magnetic intensity (TMI) grid data using standard  
 449 Euler deconvolution. This was done to locate depths to the lithology contacts on the gridded map. The  
 450 best clustering Euler depths was achieved using solution window size of 4, 1.0 structural index (SI) (steep  
 451 contact) and 15% depth tolerance. The results were plotted on the analytical signal map for effective  
 452 interpretations (Figure 9).

453  
 454



455  
 456  
 457  
 458

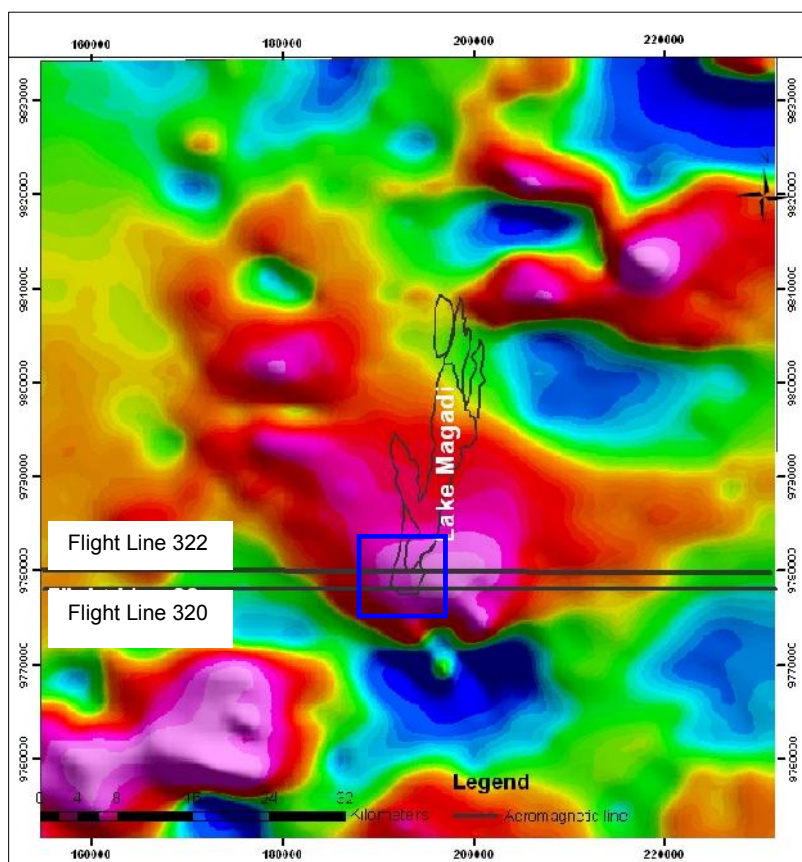
Figure 9: 3D Euler's depths solutions (structural index of 1) plotted on the colour shaded analytical signal map.

459 **2.2. Aeromagnetic Data**

460 The aeromagnetic data used in this study was part of the African Magnetic Mapping Project (AMMP),  
 461 which was intended to compile airborne magnetic data for some parts of Africa. Aeromagnetic data in the  
 462 study area was acquired by the Compagnie Generale de Geophysique (CGG) in 1987 with 2km line  
 463 spacing, flight direction of 90° (W-E) and flying height of 2896m above sea level.

465 Magnetic data on flight lines 320 and 322, covering about 7.7 km long from the total magnetic intensity  
 466 map of the aeromagnetic data are shown in Figure 10. The data processing (levelling correction and

467 geomagnetic field removal) was done by AMMP. The magnetic grid was created using 1km cell size with  
 468 AMMP grid projection system, re-projected to WGS84, UTM 37S projection later to conform to the  
 469 projection used in this study. Lake Magadi study area was clipped from the entire gridded data as shown  
 470 in Figure 10). The extracted aeromagnetic data were processed and inverted using 2D Euler  
 471 deconvolution software developed by [30] and following the same procedures and processing adopted in  
 472 the ground magnetic method. In this case, the results from IGRF 2005 model calculated from the  
 473 magnetic data were the magnetic intensity of 33414, inclination of  $-26.3^{\circ}$  and declination of  $0.002^{\circ}$  with  
 474 structural index of 1 (steep contacts). These were used as inputs to the Euler's software to construct the  
 475 subsurface magnetic sources along the selected profile lines (Figures 16 and 17).  
 476



477  
 478 Figure 10: Colour-shaded Aeromagnetic Total Magnetic Intensity (TMI)  
 479 grid data for Lake Magadi area, showing the extracted lines 322 and  
 480 320.

### 481 3. DATA INTERPRETATION

482 From the Total Magnetic Intensity (TMI) grid data, the high intensity magnetic signals at the western  
 483 margins mark the faults with basaltic rocks (Figure 6) while the eastern margin shows a decay of the  
 484 magnetic intensity corresponding to the end of the basalts and marking the onset of the chert zone. The  
 485 basin is characterized by low magnetic signatures, which can be attributed to the presence of fluids. The  
 486 two-chert zones show reasonably high magnetic anomaly in the TMI grid (Figure 6). In the vertical  
 487 derivative map (Figure 7), the hot springs, which are clearly manifested in the surface between the north-  
 488 south trending Fault A, and Fault B in the south west show low (negative) magnetic anomaly. The map  
 489 also shows the lateral continuity N-S faults along the axial rift zone. High magnetic signal within the basin  
 490 coincides with the Fault zones (B and C) (Figures 6 and 7). The analytic signal map (Figure 8) shows that  
 491 the survey area is inside a basin surrounded by the west, east Faults A and D. In this map, the edges of  
 492 the magnetic anomaly are better enhanced and it clearly shows the zones of discontinuities between

\* Tel.: +2348037899856.

E-mail address: [aakomolafe@futa.edu.ng](mailto:aakomolafe@futa.edu.ng)

493 each geologic unit, especially the major faults in the area. Majority of the hot springs occurs within a  
494 boundary between high and moderate magnetic intensity rocks. The location of hot spring is  
495 characterized by very low and negative anomaly as revealed in the vertical derivative map (Figure 7). The  
496 sediments further bury the basaltic rocks outcropping at the hot springs south; these are probably  
497 responsible for the high magnetic anomaly, which are evident in the analytical signal map (Figure 8).  
498 Within the basin is a localized high magnetic anomaly, which can be attributed to the presence of volcanic  
499 rocks. From the depth estimation, the basin depth between 300 and 493 metres, with the western and  
500 eastern basalts from the Euler's depth extending to about 300m.

501  
502  
503

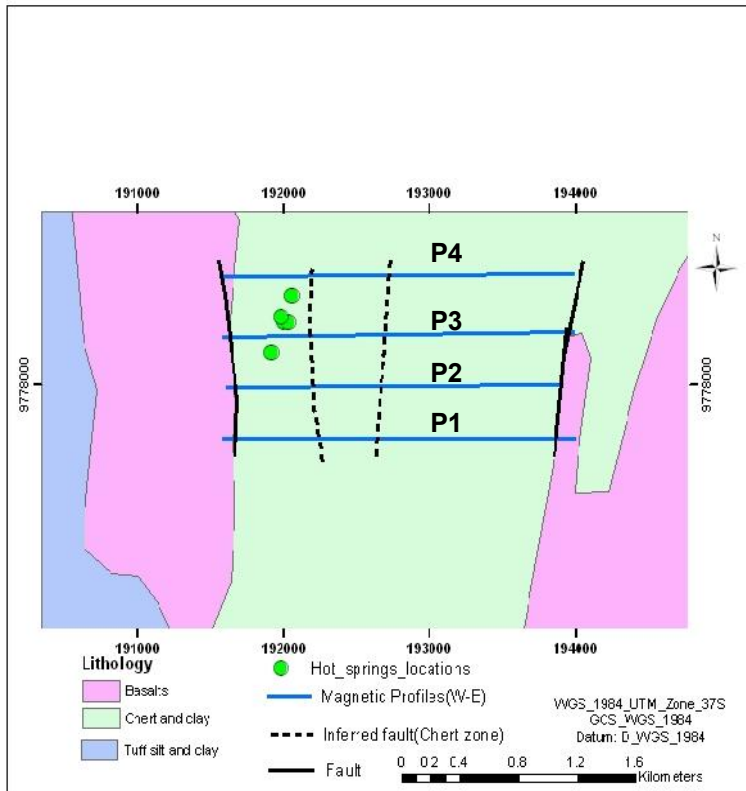
### 3.1. 2D INTERPRETATION OF THE MAGNETIC DATA ALONG THE TRAVERSES

504 Qualitative interpretation of the magnetic traverses shows that the basin is bounded by N-S trending  
505 faults both to the west and to the east. The 2D magnetic profiles (Figures 11 – 14) show the magnetic  
506 anomaly observed over the four faults in the south of Lake Magadi. The differences in magnetic anomaly  
507 signatures possibly indicate structurally controlled subsurface features [23, 31].

508 Figure 11(b) shows magnetic anomaly along traverse P1. Here, four distinct trends are recognized, which  
509 coincide with the location of the identified faults within the basin. The traverse begins with a high and low  
510 magnetic anomaly (Station 0 – 200m), which is attributed to the highly faulted basaltic dyke that bounds  
511 the basin to the west (Figure 11 a and b). This signature is followed to the east by generally low  
512 signatures (Station 200 – 380m). This very low magnetic anomaly coincides with the hot and cold spring  
513 locations within the basin. The same result was experienced in Ethiopian Rift Valley by Abiye and Tigistu  
514 [21]. The lack of magnetic sources exists mostly between the faults, an evident of the presence of fluids  
515 as experienced in the field. The discontinuity between the basalt and sediments basin show the existence  
516 of faults between the rock units. A gentle rise in the anomaly towards the east (Station 380 -500m) shows  
517 the commencement of the chert zone within Fault B followed by low signatures characterized by  
518 sediments (Station 500 -700m). The high magnetic response within this zone could be attributed to the  
519 presence of chert vein as observed in the field. At the end of the low anomaly, there is a little rise but  
520 undulating signatures (Station 700m) which commence the chert zone (Fault C), followed by a relatively  
521 low anomaly (up to Station 1700m). The eastern-most basaltic rock along the traverse shows a rise in  
522 magnetic anomaly. General fluctuation of the magnetic response along the profile and the scattering of  
523 the Euler solutions possibly indicate that series of intense tectonic/faulting activity associated with  
524 shearing might have taken place within the basin [23, 31].

525  
526

a



b.

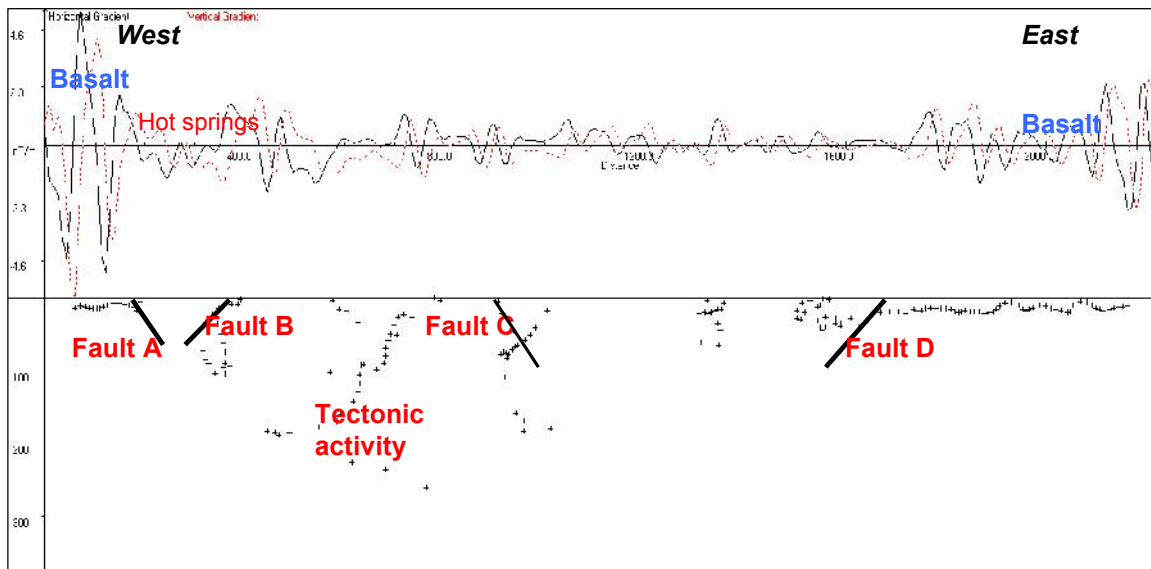
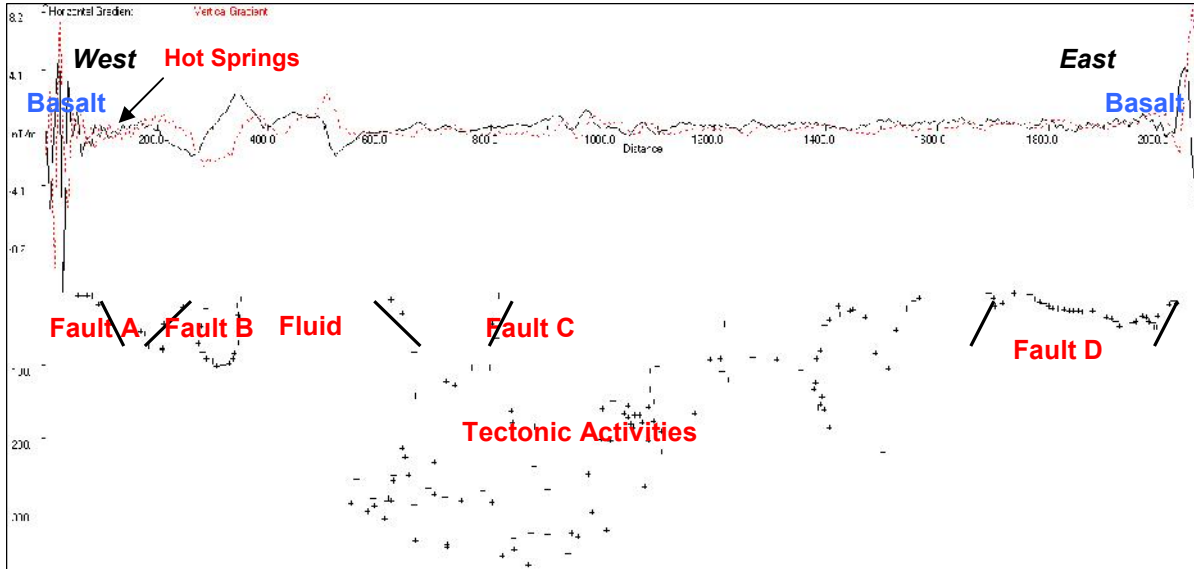


Figure 11 **a** Geologic map of the magnetic survey area. **(b)**. Processed ground magnetic data with 2-D Euler solutions obtained along traverse one with inclination and declination angles of  $-26.2^\circ$  and  $0.03^\circ$  respectively. Plus (+) signs are Euler solutions for 1.0 structural index.

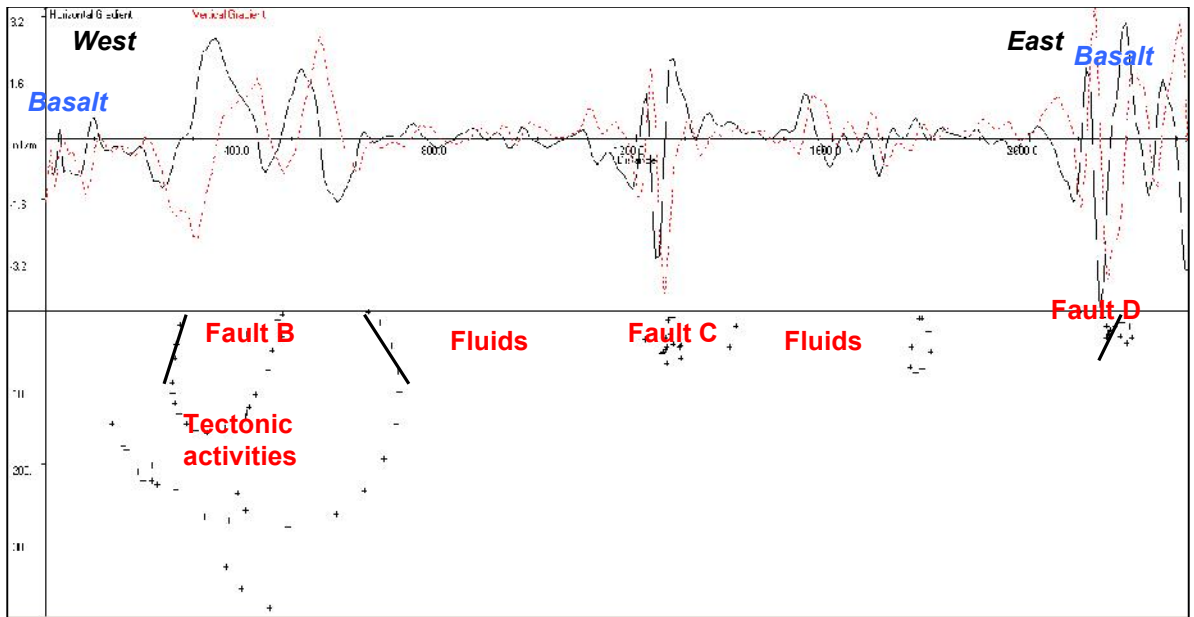
527  
 528  
 529  
 530  
 531  
 532  
 533  
 534  
 535  
 536

Traverses P2 and P3 (Figures 12 and 13) shows similar variation in magnetic signatures as traverse P1. Traverse P3 has well-defined faults, corresponding to Faults B, C, and D. The variation in magnetic amplitudes and the much scattering in the Euler solution could be attributed to an intense shearing activity and localized anomaly beneath the profiles, which is also visible in the analytical map. These scatterings are not seen in the fourth profile (Figure 14). Profile Four (P4) shows consistent high and low

537 magnetic responses along the transverse. These undulating signatures and the Euler deconvolution  
 538 solutions clearly show the subsurface faulting/contact pattern within the geological units. The subsurface  
 539 fault geometry as revealed in Traverse Four shows a general normal faulting system associated with  
 540 Magadi N-S faults. Generally in all the traverses, Faults A and D show both eastern and western dip  
 541 respectively. These faults are major structures bounding the basin in the southern part of Lake Magadi.  
 542

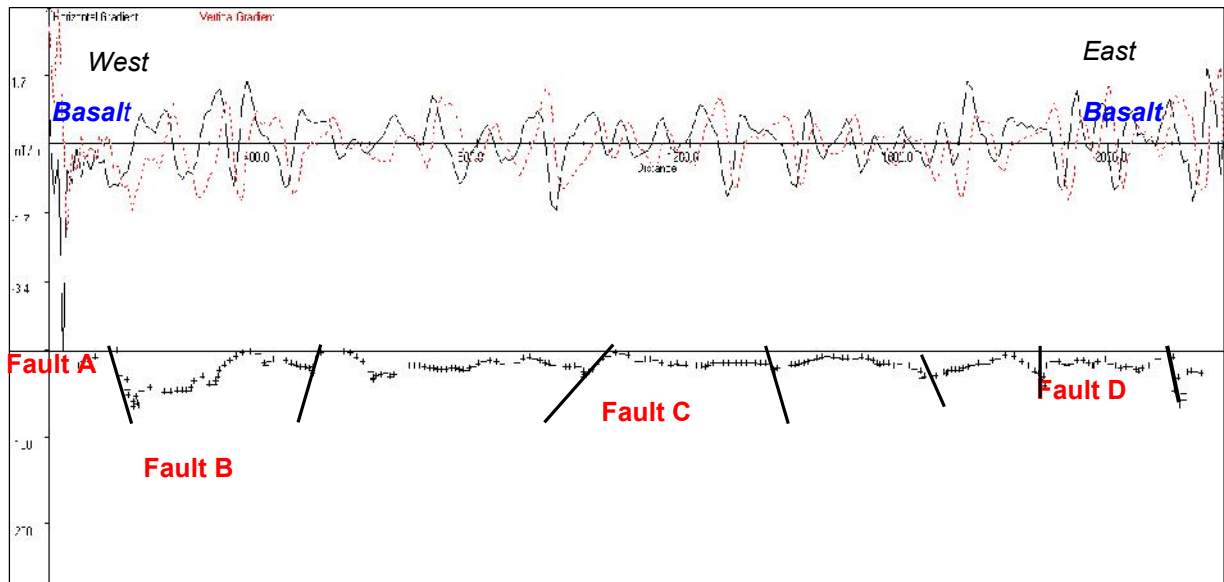


543  
 544 Figure 12. Processed ground magnetic data with 2D Euler solutions obtained along Traverse Two with  
 545 inclination and declination angles of  $-26.2^\circ$  and  $0.03^\circ$  respectively. Plus (+) signs are Euler solutions for  
 1.0 structural index.



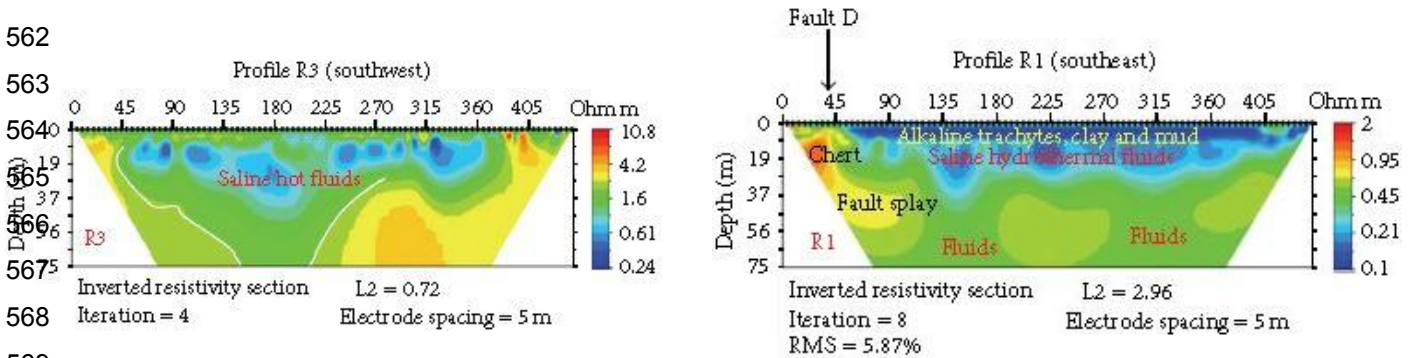
546  
 547 Figure 13. Processed ground magnetic data with 2D Euler solutions obtained along Traverse Three with  
 548 inclination and declination angles of  $-26.2^\circ$  and  $0.03^\circ$  respectively. Plus (+) signs are Euler solutions for  
 1.0 structural index.

549



550  
 551 Figure 14. Processed ground magnetic data with 2D Euler solutions obtained along Traverse Four  
 552 with inclination and declination angles of  $-26.2^\circ$  and  $0.03^\circ$  respectively. Plus (+) signs are Euler

553 Evidently, the results of the magnetic profiles confirmed the investigation done by [8] using electrical  
 554 resistivity method (Figure 15). Their resistivity profiles showed the tectonic activities up to the depth of  
 555 75m with well-defined geological units comprising faults splay both to west and east. The faults, which are  
 556 normal trending N-S are parallel faults that bounds Lake Magadi graben east and west, and they play  
 557 prominent role in the transportation of the geothermal fluid from the subsurface to the surface. The  
 558 scattering euler deconvolution in magnetic profiles confirmed the fracture zone delineated from the  
 559 geoelectric profiles as reported by Komolafe et al. [8]. The faults (A, B, C, and D) were further probed to a  
 560 deeper depth using airborne magnetic data as discussed in the next section.  
 561



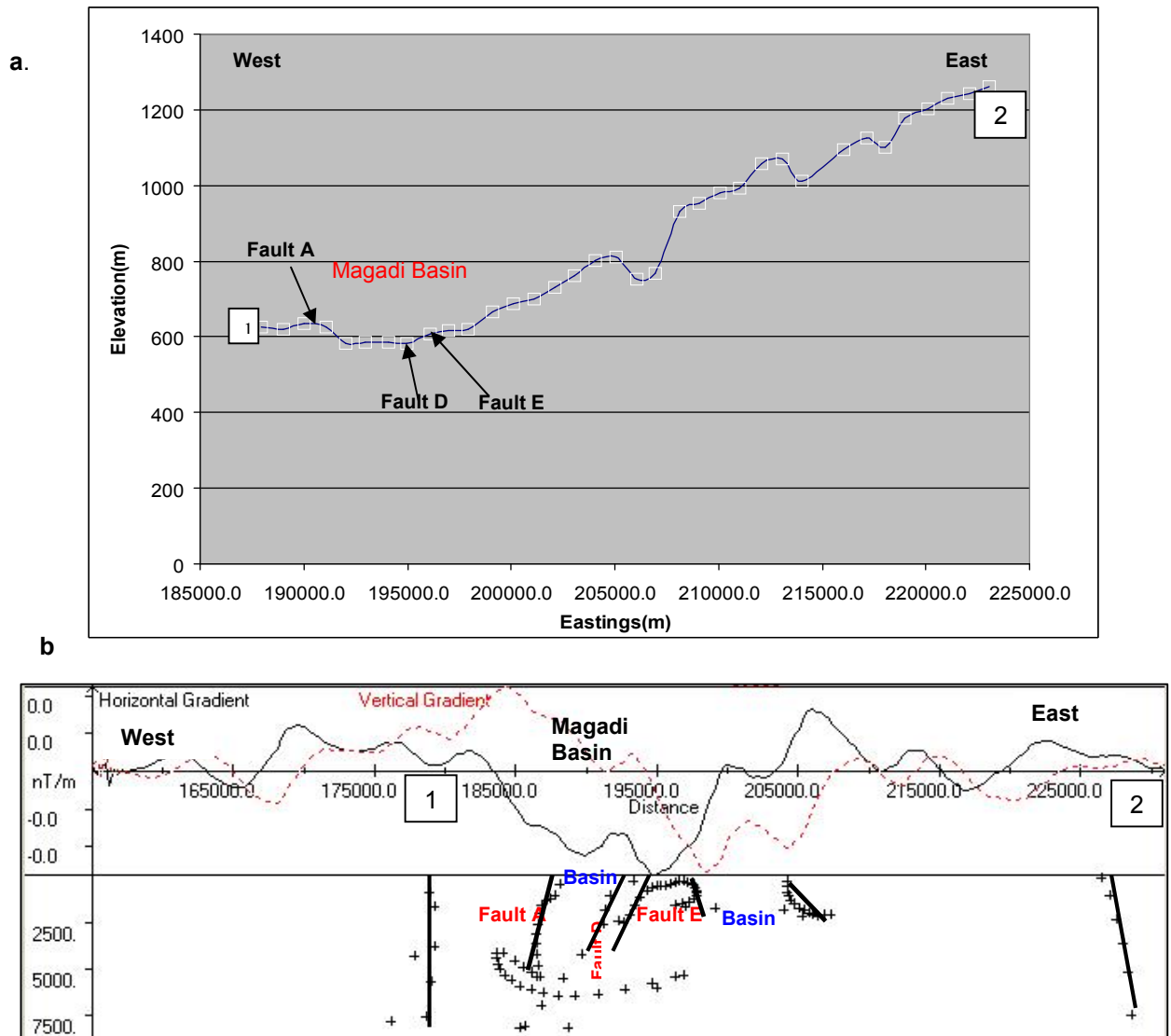
562  
 563  
 564  
 565  
 566  
 567  
 568  
 569  
 570 Figure 15 (a) Inverted 2D resistivity section for profile 3 between fault A and fault B in the southwest of  
 571 Lake Magadi (b) Inverted 2D resistivity section for profile 1 across fault D and towards fault E in the  
 572 southeast of Lake Magadi after Komolafe et al. [8].  
 573

### 574 3.2. 2D INTERPRETATION OF THE AEROMAGNETIC PROFILES

575 The processed aeromagnetic data for lines 320 and 322 are shown in Figures 16 and 17. The flight lines,  
 576 which are 2km, separated from each other shows similar subsurface geometry, both in frequency and  
 577 amplitudes. Most of the Euler solutions are concentrated along the rift axis while the basin is marked by  
 578 the absence of magnetic sources. These observations are in line with the results experienced in the  
 579 northern part of the Kenya rift by [32]. The magnetic sources from 2D Euler correspond approximately to  
 580 the top of the magnetic sources. These sources reflect rock beneath the thick sediment within the axial

\* Tel.: +2348037899856.  
 E-mail address: [aakomolafe@futa.edu.ng](mailto:aakomolafe@futa.edu.ng)

581 part of the rift basin/trough. The sub-vertical alignment and scattering of the Euler solutions reveals the  
 582 existence of tectonic activities [23, 33-34] which extends to a depth of 7.5 km (Figures 16b and 17b). The  
 583 magnetic sources correspond largely to the tectonic structures (faults). These tectonic structures,  
 584 approximately at a depth of 7.5km, correspond to the established surface N-S faults A, D and E in the  
 585 south of Lake Magadi, which bounds the basin in the surface as seen in the topographic profiles (Figure  
 586 16a and 17b). The lack of magnetic signal between the faults in the subsurface could be because of the  
 587 presence of hydrothermal fluids within the basin. Faults B and C are mostly shallow; they are not clearly  
 588 manifested in the aeromagnetic profiles, but are visible in the ground magnetic profiles.  
 589  
 590



591 Figure 16. (a) Extracted topography elevations of Lake Magadi area from Aster DEM along flight line  
 592 330 showing surface faults and grabens. (b) 2D Euler deconvolution solutions from aeromagnetic data  
 593 along flight line 320. The plus (+) signs are structural index of 1 with inclination and declinations of  $-26.3^{\circ}$   
 594 and  $0.002^{\circ}$  respectively.  
 595  
 596  
 597  
 598  
 599  
 600

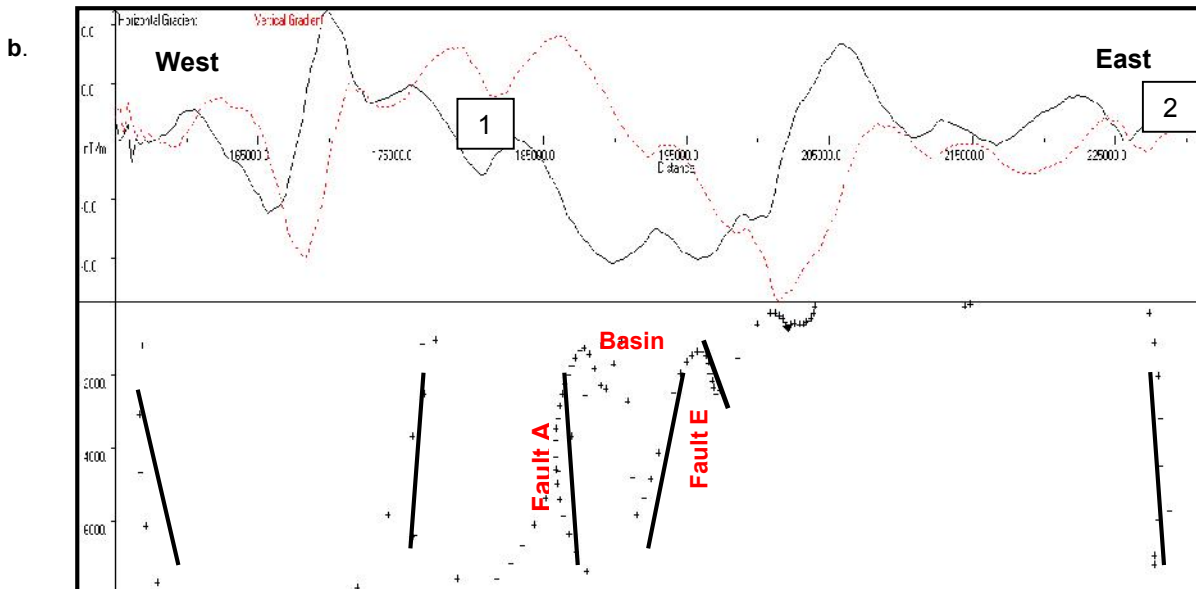
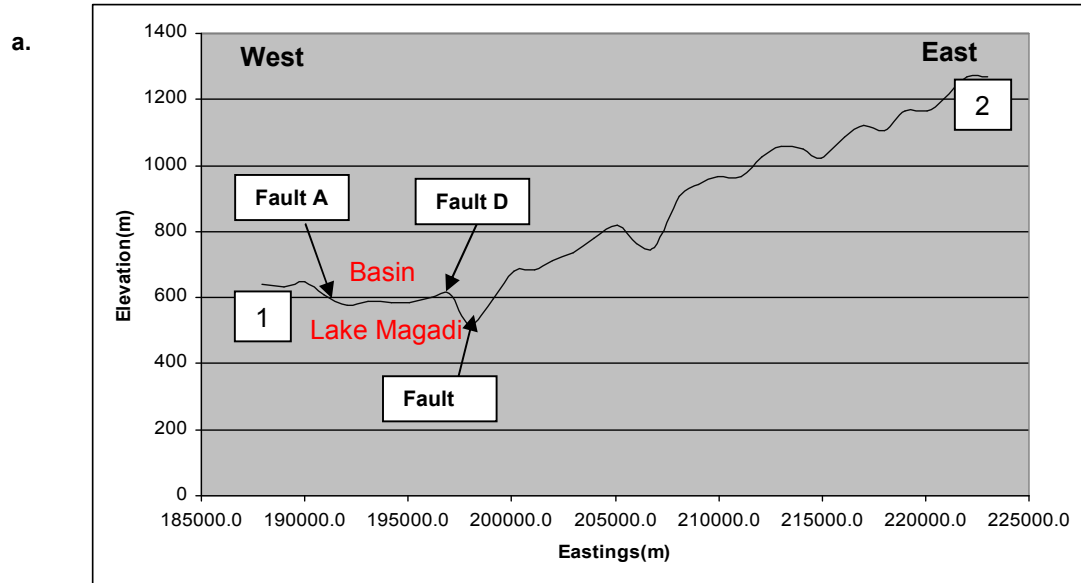


Figure 17 .(a) Extracted topography elevations of Lake Magadi area from Aster DEM along flight line 322 showing surface faults and grabens. (b) 2D Euler deconvolution solutions from aeromagnetic data along flight line 322. The plus signs are structural index of 1

601  
602  
603  
604  
605  
606

#### 6074. CONCLUSIONS

608 Detailed analysis of ground and aeromagnetic data has revealed that the Lake Magadi area is highly  
609 faulted. The multiple scattering of Euler solution in the ground magnetic profiles confirms this highly  
610 fractured and faulted zone within the subsurface. The location of the fluid filled zone within the basin is  
611 marked by the absence of magnetic source in the grids and 2D Euler's deconvolution solutions of the  
612 ground magnetic data. These fluid zones exist between the investigated tectonic lineaments as confirmed  
613 by Komolafe [8].

614  
615 This tectonic activity in the Lake Magadi upper crust contributes to the upward flow of hydrothermal fluids  
616 from the hot geothermal reservoir to the surface. It was established that the surface lineaments and

\* Tel.: +2348037899856.

E-mail address: [aakomolafe@futa.edu.ng](mailto:aakomolafe@futa.edu.ng)

617 tectonic activities along and beneath Magadi Basin extends deeply to the subsurface (approximately  
618 7.5km), with surface expressions showing as faults which bind the graben to the west and to the east. It  
619 was observed that the existence of the structures south of Lake Magadi plays an important role in  
620 creating a flow path through which the hydrothermal fluids (hot or cold) are transported to the surface.  
621 Therefore, the manifestations of hot springs and trona deposit in the south of Lake Magadi are largely  
622 supported by the presence of N-S faults in the area.  
623

## 624 ACKNOWLEDGEMENT

625  
626 Our appreciation goes to the University of Twente, ITC, Enschede, The Netherlands, and Nuffic for  
627 funding the study. We acknowledge the supports rendered by the Department of Geology, Ministry of  
628 Mineral Resources, Nairobi, Kenya for providing its Magnetometer equipment for our use. We also thank  
629 Dr Sally Barrit of the University of Twente, ITC, Enschede for the provision of aeromagnetic data.  
630

## 631 REFERENCES

- 632 1. Simiyu, S.M. and G.R. Keller, Seismic monitoring of the Olkaria Geothermal area, Kenya Rift  
633 valley. *Journal of Volcanology and Geothermal Research*, 2000. **95**(1-4): p. 197-208.
- 634 2. Gudmundsson, A., et al., Fracture networks and fluid transport in active fault zones. *Journal of*  
635 *Structural Geology*, 2001. **23**(2-3): p. 343-353.
- 636 3. Lerner, E.K.L. and B.W.L.G. Cengage. *Faults and Fractures*. 2003; Available from:  
637 <http://www.enotes.com/earth-science>.
- 638 4. Mary, H.D. and F. Mario, *What is Geothermal Energy?* 2004, Istituto di Geoscienze e Georisorse:  
639 Pisa, Italy. p. 1-61.
- 640 5. Mwaura, F., A spatio-chemical survey of hydrogeothermal springs in Lake Elementaita, Kenya.  
641 *International Journal of Salt Lake Research*, 1999. **8**(2): p. 127-138.
- 642 6. Jones, B.F., H.P. Eugster, and S.L. Rettig, Hydrochemistry of the Lake Magadi basin, Kenya.  
643 *Geochimica et Cosmochimica Acta*, 1977. **41**(1): p. 53-72.
- 644 7. Maguire, P.K.H. and R.E. Long, The Structure on the Western Flank of the Gregory Rift (Kenya).  
645 Part I. The Crust. *Geophysical Journal of the Royal Astronomical Society*, 1976. **44**(3): p. 661-  
646 675.
- 647 8. Komolafe, A.A., et al., Integrated Remote Sensing and Geophysical Investigations of the  
648 Geodynamic Activities at Lake Magadi, Southern Kenyan Rift. *International Journal of*  
649 *Geophysics*, 2012. **2012**: p. 15.
- 650 9. Stampolidis, A. and G.N. Tsokas, Curie Point Depths of Macedonia and Thrace, N. Greece. *Pure*  
651 *and Applied Geophysics*, 2002. **159**(11): p. 2659-2671.
- 652 10. Spector, A. and F.S. Grant, Statistical models for interpreting aeromagnetic data. *Geophysics*  
653 **1970**. **35**: p. 293–302.
- 654 11. Atmaoui, N. and D. Hollnack, Neotectonics and extension direction of the Southern Kenya Rift,  
655 Lake Magadi area. *Tectonophysics*, 2003. **364**(1-2): p. 71-83.
- 656 12. Eugster, H.P., Chemistry and origin of brines of Lake Magadi, Kenya. *Mineral. Soc. Amer. Spec.*  
657 *Paper*, 1970. **No. 3**: p. 215 - 235.
- 658 13. Smith, M. and P. Mosley, Crustal Heterogeneity and Basement Influence on the Development of  
659 the Kenya Rift, East Africa. *Tectonics*, 1993. **12**.
- 660 14. Baker, B.H., *Geology of the Magadi area*. 1958, Geological Survey of Kenya, Nairobi.
- 661 15. Baker, B.H., et al., Sequence and geochronology of the Kenya rift volcanics. *Tectonophysics*,  
662 1971. **11**(3): p. 191-215.
- 663 16. Sequar, G.W., Neotectonics of the East African rift system : new interpretations from conjunctive  
664 analysis of field and remotely sensed datasets in the lake Magadi area, Kenya. 2009, ITC:  
665 Enschede. p. 99.
- 666 17. Simiyu, S.M. and G.R. Keller, Upper crustal structure in the vicinity of Lake Magadi in the Kenya  
667 Rift Valley region. *Journal of African Earth Sciences*, 1998. **27**(3-4): p. 359-371.
- 668 18. Le Turdu, C., et al., Influence of pre-existing oblique discontinuities on the geometry and  
669 evolution of extensional fault patterns; Evidence from the Kenya Rift using Spot Imagery. In: C.K.  
670 Morley (Editor), *Geoscience of Rift systems-Evolution of East Africa*. AAPG studies in Geology,  
671 1999: p. 173-191.

\* Tel.: +2348037899856.

E-mail address: [aakomolafe@futa.edu.ng](mailto:aakomolafe@futa.edu.ng)

- 672 19. Jessell, M., Three-dimensional geological modelling of potential-field data. *Computers &*  
673 *Geosciences*, 2001. **27**(4): p. 455-465.
- 674 20. Clark, D.A. and D.W. Emerson, Notes on rock magnetization characteristics in applied  
675 geophysical studies. *Exploration Geophysics*, 1991. **22**(3): p. 547-555.
- 676 21. Abiye, T.A. and H. Tigistu, Geophysical exploration of the Boku geothermal area, Central  
677 Ethiopian Rift. *Geothermics*, 2008. **37**(6): p. 586-596.
- 678 22. Riddihough, R.P., Diurnal Corrections To Magnetic Surveys; An Assessment Of Errors.  
679 *Geophysical Prospecting*, 1971. **19**(4): p. 551-567.
- 680 23. Adepelumi, A.A., et al., Integrated geophysical mapping of the Ifewara transcurrent fault system,  
681 Nigeria. *Journal of African Earth Sciences*, 2008. **52**(4-5): p. 161-166.
- 682 24. Briggs, I.C., Machine Contouring Using Minimum Curvature. *GEOPHYSICS*, 1974. **39**(1): p. 39-  
683 48.
- 684 25. Cooper, G.R.J. and D.R. Cowan, Filtering using variable order vertical derivatives. *Computers &*  
685 *Geosciences*, 2004. **30**(5): p. 455-459.
- 686 26. Roest, W.R., J. Verhoef, and M. Pilkington, Magnetic interpretation using the 3-D analytic signal.  
687 *Geophysics* 1992. **57**: p. 116–125.
- 688 27. Jeng, Y., et al., Integrated signal enhancements in magnetic investigation in archaeology. *Journal*  
689 *of Applied Geophysics*, 2003. **53**(1): p. 31-48.
- 690 28. MacLeod, I.N., K. Jones, and T.F. Dai, 3-D analytic signal in the interpretation of total magnetic  
691 field data at low magnetic latitudes. *Exploration Geophysics*, 1993. **24**(4): p. 679-688.
- 692 29. El Dawi, M.G., et al., Depth estimation of 2-D magnetic anomalous sources by using Euler  
693 deconvolution method. *American Journal of Applied Sciences* 2004.
- 694 30. Cooper, G.R.J., Euler deconvolution applied to potential field gradients. *Exploration Geophysics*,  
695 2004. **35**(3): p. 165-170.
- 696 31. Telford, W.M., L.P. Geldart, and R.E. Sheriff, *Applied Geophysics*. second ed. Vol. 1. 1976:  
697 Cambridge University Press. 50-102.
- 698 32. Mariita, N.O. and G.R. Keller, An integrated geophysical study of the northern Kenya rift. *Journal*  
699 *of African Earth Sciences*, 2007. **48**(2-3): p. 80-94.
- 700 33. Mushayandebvu, M.F., et al., Magnetic source parameters of two-dimensional structures using  
701 extended Euler deconvolution. *Geophysics*, 2001. **66**(3): p. 814-823.
- 702 34. Kuria, Z.N., et al., Active fault segments as potential earthquake sources: Inferences from  
703 integrated geophysical mapping of the Magadi fault system, southern Kenya Rift. *Journal of*  
704 *African Earth Sciences*, 2010. **57**(4): p. 345–359.
- 705
- 706